INTERNATIONAL JOURNAL FOR NUMERICAL AND ANALYTICAL METHODS IN GEOMECHANICS
Int. J. Numer. Anal. Meth. Geomech., 2000; **24**:627–653

Performance of displacement finite elements for modelling incompressible materials

H. S. Yu*,† and M. D. Netherton

Department of Civil, Surveying and Environmental Engineering, The University of Newcastle, N.S.W. 2308, Australia

SUMMARY

It is well established that severe numerical difficulties may arise when the displacement finite element method is used to analyse the behaviour of incompressible solids and this is particularly true for axisymmetric problems. These numerical difficulties are caused by excessive kinematic constraints and are reflected by strong oscillations in the calculated stress distribution and overestimations of collapse loads. The purpose of this paper is to present new displacement finite element formulations which are particularly suitable for axisymmetric analysis of incompressible materials. A direct comparison is made of the performance of various displacement finite elements in the analysis of elastic or plastic incompressible materials under axisymmetric loading conditions. Particular attention is focused on the performance of various axisymmetric displacement elements in predicting the stress field of incompressible or nearly incompressible materials.

KEY WORDS: finite elements; incompressible materials; elasticity; plasticity; stress analysis; soil mechanics

INTRODUCTION

It is well known that finite element analysis of undrained geotechnical problems has encountered severe numerical difficulties over the years. One notable example is that the conventional displacement finite element method suffers from the disadvantages that the accuracy of the calculated stresses reduced dramatically as the compressibility approaches zero. This phenomenon, which is widely known as 'locking', has been reported in the literature by many researchers (see, for example, [1–6]).

In 1974, Nagtegaal *et al.* [4] published a landmark paper on the theoretical analysis of the difficulties associated with finite element calculations in the fully plastic range involving incompressible behaviour. By considering the limiting case of a very fine mesh, they proved that most displacement finite elements which employ low-order polynomials to model the displacement field are not suitable for incompressibility computations, and this is particularly true for axisymmetric problems. This is because the incremental incompressibility condition typically imposes a large number of constraints on the nodal velocities which, effectively, reduces the

*Correspondence to: H. S. Yu, Department of Civil, Surveying and Environmental Engineering, The University of Newcastle, N.S.W. 2308, Australia
†Associate Professor

Received 30 January 1999
Revised 6 October 1999

available number of degrees of freedom. Since these constraints may multiply at a faster rate than the new degrees of freedom as the mesh is refined, it may not be possible to ensure that there are sufficient degrees of freedom available to accommodate the constant volume condition, regardless of how many elements are used in the grid.

One of the earlier approaches used to overcome this problem is the reduced integration rule suggested by Zienkiewicz *et al.* [5]. The typical element used in this type of approach is the 8-noded rectangle with 4-point integration. As discussed by Naylor [3] and Sloan and Randolph [7], reduced integration has the beneficial effect of decreasing the total number of incompressibility constraints on the nodal degrees of freedom. This is clearly seen by noting that the maximum number of constraints per element must be less than, or equal to, the total number of integration points used in the calculation of the element stiffness matrices. A theoretical justification of using reduced integration in analysing incompressible materials has been given by Malkus and Hughes [8]. They proved that displacement formulations with reduced integration are, in certain cases, equivalent to mixed formulations where both stresses and displacements are treated as variables. This equivalence typically holds in plane strain and three-dimensional analysis. However, the equivalence breaks down for the case of axisymmetric loading.

Although it was once widely used in the finite element community, the reduced integration method can produce spurious stress and displacement oscillations and this is caused by the formation of zero-energy modes. To illustrate the limitations of the reduced integration method, Sloan and Randolph [9] presented a number of numerical examples on footings and vertical cuts in which the reduced integration approach leads to incorrect or unacceptable deformation predictions. In particular, the initial and deformed meshes shown in Sloan and Randolph [9] for a rigid circular footing that were obtained using the reduced integration method indicate that the finite elements in the vicinity of the footing deform in a bulging mode and numerical problems are clearly evident. Recently, Naylor [10] also demonstrated that even a high-order element (cubic triangles), when used with six integration points (reduced integration), produces a zero-energy mechanism. These shortcomings are relatively well known in the area of computational geomechanics and a number of other important cases have also been discussed by Sloan [11], and De Borst and Vermmer [12] among others. At a more fundamental level, the major limitation of using the reduced integration technique is that the incompressibility condition is satisfied only at a limited number of integration points, rather than everywhere within the element. In other words, even though reduced integration may give reasonably accurate stress prediction at a limited number of integration points within an element, the numerical stress field in the remaining part of the element would be highly incorrect.

Another method for the analysis of incompressible materials, which does not have the drawbacks associated with reduced integration, is to use a high-order element as suggested by Sloan and Randolph [7]. Using the analysis of Nagtegaal *et al.* [4], they proved that high-order elements can provide a sufficient number of degrees of freedom to satisfy the constant volume condition. This is so because the number of degrees of freedom per element increases faster than the number of incompressibility constraints when the order of an element increases. According to Sloan [11], the lowest order of triangular element for axisymmetric problems suitable for this approach is a 15-noded cubic strain element. Although this approach works well, it suffers from the drawback that the high-order elements cause a large bandwidth in the stiffness matrix, which may require some sophisticated equation solvers.

More recently, Yu [13,14] has proved that the number of incompressibility constraints may also be reduced by choosing appropriate displacement interpolation functions. In particular, Yu

[13,14] proposed a modified displacement interpolation function which can be used to develop suitable displacement finite elements for axisymmetric analysis of incompressible materials. The application of this new displacement interpolation function to a six-noded triangular element presented by Yu *et al.* [15] suggests that this novel approach permits low-order elements to be successfully used for axisymmetric analysis of incompressible materials. Yu's new formulation is also simple to implement in a standard finite element program. Since Yu's approach employs full integration to evaluate the element stiffness matrices, the numerical examples (including footing problems) presented in Yu [13,14] and Yu *et al.* [15] show that no problems are experienced with barrelling or zero-energy mechanisms. It is noted that Yu's displacement interpolation function has also been used successfully by Jinka and Lewis [16] to develop a modified mixed and penalty formulation for axisymmetric analysis of incompressible materials.

Although in theory Yu's displacement interpolation function can be applied to all types of displacement finite elements, so far it has only been implemented into the six-noded triangular element. A major objective of this paper is therefore to present a general finite element formulation which can be used to implement Yu's displacement interpolation function in any type of displacement elements. Further, in this study, we have also detailed the way by which the new formulations of 3-, 6-, 10- and 15-noded triangular elements and 4-, 8-noded quadrilateral elements can be implemented in a standard displacement finite element program. The performance of these new elements will be investigated by comparing the numerical results with exact solutions.

THEORY

Plane strain loading conditions

To illustrate the difficulties associated with the analysis of incompressible materials, consider the eight-noded rectangle shown in Figure 1. The conventional displacement interpolation function for this element is given by

$$\dot{u} = c_1 + c_2x + c_3y + c_4x^2 + c_5xy + c_6y^2 + c_7x^2y + c_8xy^2 \tag{1}$$

$$\dot{v} = c_9 + c_{10}x + c_{11}y + c_{12}x^2 + c_{13}xy + c_{14}y^2 + c_{15}x^2y + c_{16}xy^2 \tag{2}$$

where $\dot{u}$ and $\dot{v}$ are the velocities in the x- and y-directions, and $c_1, c_2, \ldots, c_{16}$ are unknown coefficients which are functions of the nodal velocities and the nodal co-ordinates.

Under the conditions of plane strain, the incremental constant volume condition may be written as

$$\frac{\partial \dot{u}}{\partial x} + \frac{\partial \dot{v}}{\partial y} = 0 \tag{3}$$

Substituting (1) and (2) into (3) gives another form of the incompressibility condition

$$(c_2 + c_{11}) + (2c_4 + c_{13})x + (c_5 + 2c_{14})y + (2c_7 + 2c_{16})xy + c_{15}x^2 + c_8y^2 = 0 \tag{4}$$

In the displacement finite element method, the element stiffness matrices and stresses are normally evaluated at a discrete number of integration points. The number of integration points used in each element is denoted by N_g. For the 8-noded rectangle a 9-point integration rule

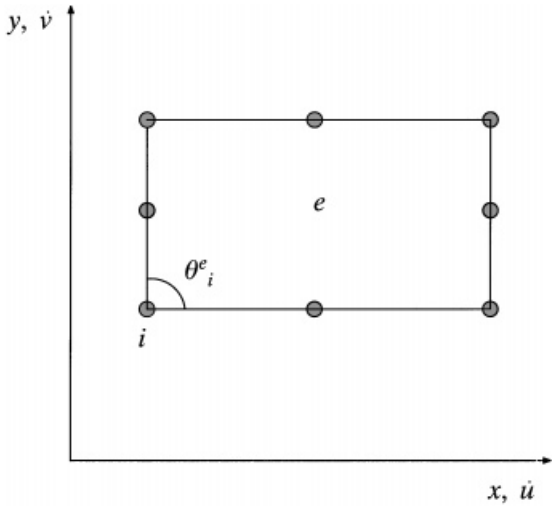

Figure 1. A 8-noded rectangle in plane strain.

(i.e. $N_g = 9$), which is generally regarded as 'full integration', should be employed. This means that Equation (4) must be satisfied as nine independent locations within the element. Using the method suggested by Sloan (1981), it may easily be shown that satisfaction of (4) at 9 independent locations imposes six incompressibility constraints on the nodal degrees of freedom. These constraints are

$$(c_2 + c_{11}) = (2c_4 + c_{13}) = (c_5 + 2c_{14}) = (2c_7 + 2c_{16}) = c_{15} = c_8 = 0 \tag{5}$$

The above analysis, which is valid for the 8-noded rectangle under conditions of plane strain, may be extended to axisymmetric loading and other types of elements. For the Lagrange family of elements, Sloan [11] has derived formulae which give the maximum number of constraints per element, c_e, arising from the incompressibility condition. These are shown in Table I and are expressed in terms of N, the order of the highest complete polynomial in the velocity expansion. Unfortunately, similar formulae for the serendipity family of elements are not readily apparent due to the *ad hoc* nature in which the high-order terms are accumulated as the element order is increased.

For an element to be suitable for modelling incompressible behaviour, it must have a sufficient number of degrees of freedom to satisfy the incompressibility constraints. Following Nagtegaal *et al.* [4], the suitability of a particular type of element may be determined by considering the limiting case of a very fine mesh to find the number of degrees of freedom per constraint. This ratio, which must be greater than or equal to 1 for good performance, is given as f_e/c_e, where f_e is the limiting value of degrees of freedom per element. The quantity f_e is defined uniquely for each type of element, regardless of the mesh arrangement, according to

$$f_e = \frac{1}{\pi} \sum_{i=1}^{i=n} \theta_i^e \tag{6}$$

Table I. Formulae for the number of incompressibility constraints per element c_e.

	Lagrangian rectangles	Lagrangian triangles
Plane strain	$N(N+2)$	$0.5N(N+1)$
Axisymmetric	$N(N+3)+1$	$0.5(N+1)(N+2)$

where θ_i^e represents the internal angle for node i of element e and n is the number of nodes per element.

For the 8-noded rectangle, from (5) and (6) we can see that $c_e = 6$ and $f_e = 6$. Hence the number of degrees of freedom per constraint in the limiting case of a very fine mesh is equal to $f_e/c_e = 6/6 = 1$. Since this value is not less than 1, the 8-noded rectangle is deemed to be suitable for analysis of incompressible behaviour under plane strain conditions.

Axisymmetric loading conditions

For axisymmetric loading, let us consider the 8-noded rectangle shown in Figure 2. Following the usual convention of using (r, z) to denote the co-ordinates of axisymmetric problems, the conventional displacement interpolation function for axisymmetric version of this element is as follows:

$$\dot{u} = c_1 + c_2 r + c_3 z + c_4 r^2 + c_5 rz + c_6 z^2 + c_7 r^2 z + c_8 r z^2 \tag{7}$$

$$\dot{v} = c_9 + c_{10} r + c_{11} z + c_{12} r^2 + c_{13} rz + c_{14} z^2 + c_{15} r^2 z + c_{16} r z^2 \tag{8}$$

where $\dot{u}$ and $\dot{v}$ are the velocities in the r- and z-directions, and $c_1, c_2, \ldots, c_{16}$ are unknown coefficients which are functions of the nodal velocities and the nodal co-ordinates.

Under the conditions of axisymmetry, the incremental constant volume condition may be written as follows:

$$\frac{\partial \dot{u}}{\partial r} + \frac{\partial \dot{v}}{\partial z} + \frac{\dot{u}}{r} = 0 \tag{9}$$

By substituting (7) and (8) into (9), we obtain the following incompressibility condition:

$$(2c_2 + c_{11}) + (3c_4 + c_{13})r + (2c_5 + 2c_{14})z + (3c_7 + 2c_{16})rz + c_{15} r^2 + 2c_8 z^2 + c_1 \frac{1}{r} + c_3 \frac{z}{r} + c_6 \frac{z^2}{r} = 0 \tag{10}$$

If 9-point integration is used to evaluate the element stiffness, then equation (10) imposes the following constraints on the nodal velocities:

$$(2c_2 + c_{11}) = (3c_4 + c_{13}) = (2c_5 + 2c_{14}) = (3c_7 + 2c_{16}) = c_{15} = 2c_8 = c_1 = c_3 = c_6 = 0 \tag{11}$$

This gives nine constraints for each element, i.e. $c_e = 9$. On the other hand, the number of degrees of freedom per element is $f_e = 6$. Hence, the limiting number of degrees of freedom per constraint, with a 9-point integration (i.e. full integration), is equal to the unacceptable low value of $f_e/c_e = 6/9 = 0.67$. According to the criterion of Nagtegaal *et al.* [4], the 8-noded rectangle with

Table II. Suitability of plane strain and axisymmetric elements for incompressible analysis with full integration.

Element type		Plain strain				Axisymmetric			
	f_e	N_g	c_e	f_e/c_e	Suitable	N_g	c_e	f_e/c_e	Suitable
3-noded triangle	1	1	1	1	Yes	3	3	1/3	No
6-noded triangle	4	3	3	4/3	Yes	6	6	2/3	No
10-noded triangle	9	6	6	3/2	Yes	12	10	9/10	No
15-noded triangle	16	12	10	8/5	Yes	16	15	16/15	Yes
4-noded rectangle	2	4	3	2/3	No	9	5	2/5	No
8-noded rectangle	6	9	6	1	Yes	9	9	2/3	No

a full integration rule is not suitable for analysis of incompressible materials under axisymmetric loading conditions.

The above analysis can be applied to all types of displacement elements to assess their suitability for modelling incompressible materials. Table II presents the results derived by Sloan [11] on the suitability of some triangular and rectangular elements under both plane strain and axisymmetric conditions.

As the number of incompressibility constants per element must be less than or equal to the number of integration points used to evaluate the element stiffness matrices, the integration rule has a direct effect on the limiting ratio of degrees of freedom to constraints. In Table II, the integration rules have been selected so that the stiffness for an elastic element with straight sides is evaluated exactly under conditions of plane strain. This is generally referred to as 'full integration' rather than 'exact integration', since it is generally not possible to compute the stiffness exactly for an element with curved sides. Due to the presence of hoop strain terms, none of the schemes can evaluate the element stiffness exactly for axisymmetric problems. To ensure that the element stiffness can be calculated accurately, most finite element codes use the same order or a slightly higher order of integration rule than that for plane strain (e.g. [17]).

THE USE OF NEW DISPLACEMENT INTERPOLATION FUNCTIONS

The results presented in Table II indicate that although all the displacement elements (with exception of the 4-noded rectangle) are suitable for plane strain problems, they are generally not suited for analysis of axisymmetric problems. There is only one element that is found to be suitable for axisymmetric incompressible analysis and that is the 15-noded cubic triangular element. This has led Sloan and Randolph [7] to propose the use of high-order elements for analysis of incompressible materials under both plane strain and axisymmetric loading conditions.

As an alternative to using high-order elements, Yu [13,14] has proposed the use of a new interpolation function. This reduces the number of incompressibility constraints on the nodal degrees of freedom and permits low-order elements to be used successfully. To illustrate this approach, once again we will consider the axisymmetric 8-noded rectangle shown in Figure 2.

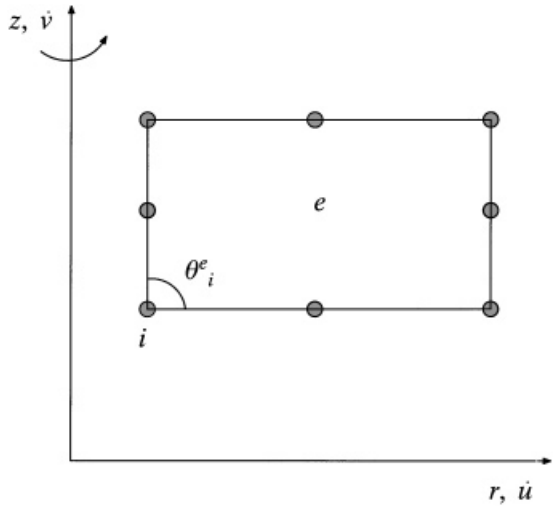

Figure 2. A 8-noded rectangle in axisymmetry.

Comparing the incompressibility condition (3) for plane strain conditions, and (9) for axisymmetric conditions, it may be seen that the three additional constraints imposed in the axisymmetric formulation are caused by the additional hoop strain term. As shown in Yu [13, 14], these additional constraints may be removed if the formulation is based on the generalized radial co-ordinate R and its velocities $\dot{R}$, which satisfy the following condition:

$$\frac{\partial \dot{R}}{\partial R} = \frac{\partial \dot{u}}{\partial r} + \frac{\dot{u}}{r} = \frac{\partial \dot{r}}{\partial r} + \frac{\dot{r}}{r} = 0 \tag{12}$$

The incompressibility condition for axisymmetric cases, equation (9), may now be cast in the same form as the incompressibility condition for plane strain:

$$\frac{\partial \dot{R}}{\partial R} + \frac{\partial \dot{z}}{\partial z} = 0 \tag{13}$$

If the formulation is based on the use of a 8-noded rectangular element, then the expansion for the velocities should be

$$\dot{U} = \dot{R} = c_1 + c_2 R + c_3 z + c_4 R^2 + c_5 Rz + c_6 z^2 + c_7 R^2 z + c_8 R z^2 \tag{14}$$

$$\dot{v} = \dot{z} = c_9 + c_{10} R + c_{11} z + c_{12} R^2 + c_{13} Rz + c_{14} z^2 + c_{15} R^2 z + c_{16} R z^2 \tag{15}$$

By substituting (14) and (15) into the incompressibility condition (13), it may easily be shown that the number of incompressibility constraints is $c_e = 6$, rather than 9 that is obtained if the conventional displacement interpolation function is used. Equation (12) can be solved to give solutions for the generalized radial co-ordinate R and its velocity $\dot{R}$ as follows:

$$R = r^2, \quad \dot{R} = \dot{U} = 2\dot{r}r = 2\dot{u}r \tag{16}$$

Table III. Suitability of modified and conventional axisymmetric elements for incompressible analysis with full integration.

Element type		Axisymmetric (new displacement interpolation)				Axisymmetric (conventional interpolation)			
	f_e	N_g	c_e	f_e/c_e	Suitable	N_g	c_e	f_e/c_e	Suitable
3-noded triangle	1	3	1	1	Yes	3	3	1/3	No
6-noded triangle	4	6	3	4/3	Yes	6	6	2/3	No
10-noded triangle	9	12	6	3/2	Yes	12	10	9/10	No
15-noded triangle	16	16	10	8/5	Yes	16	15	16/15	Yes
4-noded rectangle	2	9	3	2/3	No	9	5	2/5	No
8-noded rectangle	6	9	6	1	Yes	9	9	2/3	No

Following the above analysis for other displacement finite elements, we can derive new set of values of the limiting ratio of degrees of freedom per constraint when the new displacement interpolation functions are used. The results of such an analysis are summarized in Table III. It is found that all the elements (with exception of the 4-noded rectangle) are suitable for axisymmetric analysis of incompressible materials provided the new displacement interpolation functions are used.

In summary, it has been found that if the 'full integration' is used most displacement finite elements (with an exception of the 15-noded triangular element) fail to satisfy the suitability criterion of Nagtegaal *et al.* [4] for axisymmetric loading conditions, and therefore are not suitable for axisymmetric analysis of incompressible materials. Using the 8-noded rectangle as an example, it has been demonstrated that the problem can be removed by using the generalized radial co-ordinate and its velocities in the finite element formulation.

FINITE ELEMENT FORMULATIONS

Yu [13] and Yu *et al.* [15] have proposed two alternative formulations of 6-noded triangular elements that can be used to implement the new displacement interpolation function into a standard finite element code. To minimize the modifications to the standard finite element code, this paper will focus on the procedure in which the conventional displacement variables are retained but modifications are made to the shape functions. Figure 3 shows an example element (e.g. 3-noded triangular element) plotted in the original co-ordinates (r, z), the generalized co-ordinates (R, z), and the area coordinates (α, β).

The strain rate–velocity relationship

The velocity field vector, $\mathbf{u}$, is defined in the conventional way:

$$\mathbf{u} = [\dot{r}, \dot{z}]^{\mathrm{T}} = [\dot{u}, \dot{v}]^{\mathrm{T}} \tag{17}$$

The strain rate vector, ε, is written in terms of the velocity vector:

$$\boldsymbol{\varepsilon} = [\dot{\varepsilon}_r, \dot{\varepsilon}_z, \dot{\gamma}_{rz}, \dot{\varepsilon}_\theta]^{\mathrm{T}} = \mathbf{L}_n \mathbf{u} \tag{18}$$

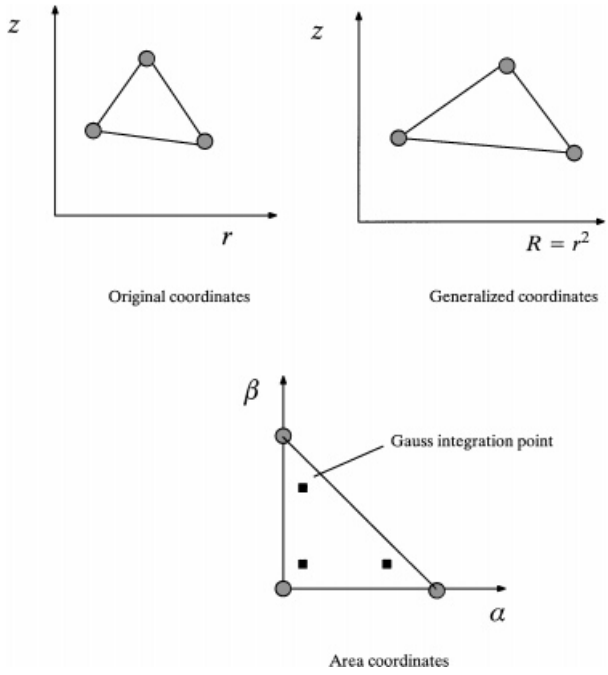

Figure 3. Mapping of a 3-noded triangular element.

where the linear operator matrix $\mathbf{L}_n$ is

$$\mathbf{L}_n = \begin{bmatrix} \dfrac{\partial}{\partial r} & 0 \\ 0 & \dfrac{\partial}{\partial z} \\ \dfrac{\partial}{\partial z} & \dfrac{\partial}{\partial r} \\ \dfrac{1}{r} & 0 \end{bmatrix} \tag{19}$$

The strain rate–nodal velocity relationship

The conventional nodal velocity vector, $\mathbf{a}^e$, is retained:

$$\mathbf{a}^e = [\dot{u}_1, \dot{v}_1, \ldots, \dot{u}_{\mathrm{nd}}, \dot{v}_{\mathrm{nd}}]^{\mathrm{T}} \tag{20}$$

where nd is the number of nodes per element.

The proposed new displacement interpolation function can be used to relate the velocity field vector $\mathbf{u}$ to the nodal velocity vector $\mathbf{a}^e$ as follows:

$$\mathbf{u} = \mathbf{N}_n \mathbf{a}^e \tag{21}$$

where the general new shape function matrix $\mathbf{N}_n$, which is valid for all element types, can be derived as

$$\mathbf{N}_n = \begin{bmatrix} \bar{N}_1 & 0 & \cdots & \bar{N}_{\mathrm{nd}} & 0 \\ 0 & N_1 & \cdots & 0 & N_{\mathrm{nd}} \end{bmatrix} \tag{22}$$

and

$$\bar{N}_i = \frac{N_i r_i}{r} \tag{23}$$

where N_i is the conventional shape function at node i; $\bar{N}_i$ the modified shape function at node i; r_i the radius of node i; and r the radius of integration points.

Substituting equation (21) into (18) results in

$$\boldsymbol{\varepsilon} = \mathbf{L}_n \mathbf{u} = \mathbf{L}_n \mathbf{N}_n \mathbf{a}^e = \mathbf{B}_n \mathbf{a}^e \tag{24}$$

where the general new strain rate-nodal velocity matrix $\mathbf{B}_n$ which is valid for all element types is as follows:

$$\mathbf{B}_n = \begin{bmatrix} \dfrac{\partial \bar{N}_1}{\partial r} & 0 & \cdots & \dfrac{\partial \bar{N}_{\mathrm{nd}}}{\partial r} & 0 \\ 0 & \dfrac{\partial N_1}{\partial z} & \cdots & 0 & \dfrac{\partial N_{\mathrm{nd}}}{\partial z} \\ \dfrac{\partial \bar{N}_1}{\partial z} & \dfrac{\partial N_1}{\partial r} & \cdots & \dfrac{\partial \bar{N}_{\mathrm{nd}}}{\partial z} & \dfrac{\partial N_{\mathrm{nd}}}{\partial r} \\ \dfrac{\bar{N}_1}{r} & 0 & \cdots & \dfrac{\bar{N}_{\mathrm{nd}}}{r} & 0 \end{bmatrix} \tag{25}$$

where

$$\frac{\bar{N}_i}{r} = r_i \frac{N_i}{R} \tag{26}$$

$$\frac{\partial \bar{N}_i}{\partial z} = \frac{r_i}{r} \frac{\partial N_i}{\partial z} \tag{27}$$

$$\frac{\partial \bar{N}_i}{\partial r} = -r_i \frac{N_i}{R} + 2 r_i \frac{\partial N_i}{\partial R} \tag{28}$$

The nodal force–nodal velocity relationship

The application of the principle of virtual displacement to an element in the original co-ordinates (r, z) can be used to give the following nodal force–nodal velocity relationship, which may be expressed in terms of the variables in the generalized co-ordinates (R, z) as follows:

$$\dot{\mathbf{P}}^e = \pi \iint_{V^e} \mathbf{B}_n^{\mathrm{T}} \dot{\boldsymbol{\sigma}} \, \mathrm{d}R \, \mathrm{d}z = \mathbf{K}_n \mathbf{a}^e \tag{29}$$

where the nodal force vector is defined by

$$\dot{\mathbf{P}}^e = [(2\pi r p_h)_1, (2\pi r p_v)_1, \ldots, (2\pi r p_h)_{\mathrm{nd}}, (2\pi r p_v)_{\mathrm{nd}}]^{\mathrm{T}} \tag{30}$$

in which p_h and p_v represent nodal force increments per unit length in radial and axial directions, respectively. The element stiffness matrix $\mathbf{K}_n$ is given by

$$\mathbf{K}_n = \pi \iint_{(\alpha,\beta)} \mathbf{B}_n^{\mathrm{T}} \mathbf{D}^{\mathrm{ep}} \mathbf{B}_n \det J \, \mathrm{d}\alpha \, \mathrm{d}\beta \tag{31}$$

where $\mathbf{D}^{\mathrm{ep}}$ is the elastic–plastic stress strain matrix and J is the Jacobian of the transformation from (R, z) to (α, β) co-ordinates.

The nodal force vectors

Following the procedure of Yu [13] and Yu *et al.* [15] for the 6-noded triangle, we can derive the general expressions for the following three types of nodal force vectors that are valid for all axisymmetric displacement elements.

Residual stresses. By using equation (29), the element nodal force vector due to a residual stress vector $\boldsymbol{\sigma}_0$ is

$$\mathbf{P}_{\boldsymbol{\sigma}_0}^e = \pi \iint_{(\alpha,\beta)} \mathbf{B}_n^{\mathrm{T}} \boldsymbol{\sigma}_0 \det J \, \mathrm{d}\alpha \, \mathrm{d}\beta \tag{32}$$

Body forces. The body forces per unit volume in the radial and axial directions are defined by b_r and b_z respectively. The corresponding nodal force vector is obtained by applying the virtual work principle to an element:

$$\mathbf{P}_b^e = \pi \iint_{(\alpha,\beta)} \mathbf{N}_n^{\mathrm{T}} \mathbf{b} \det J \, \mathrm{d}\alpha \, \mathrm{d}\beta \tag{33}$$

where the body force vector $\mathbf{b} = [b_r, b_z]^{\mathrm{T}}$.

Surface tractions. Applying the virtual displacement principle to an element such as the one shown in Figure 4, the equivalent nodal force vector may be shown to be

$$\mathbf{P}_s^e = 2\pi \int_{\xi} \mathbf{N}_n^{\mathrm{T}} r \begin{bmatrix} \dfrac{q}{2r}\dfrac{\partial R}{\partial \xi} - p\dfrac{\partial z}{\partial \xi} \\ q\dfrac{\partial z}{\partial \xi} + \dfrac{p}{2r}\dfrac{\partial R}{\partial \xi} \end{bmatrix} \mathrm{d}\xi \tag{34}$$

where the shape function matrix $\mathbf{N}_n$ depends on element types and the number of nodes per side for the element upon which the surface traction is applied. ξ is the one-dimensional co-ordinate along the loaded element side whose values are zero at the middle point of the element side, and -1 and $+1$ at two end points.

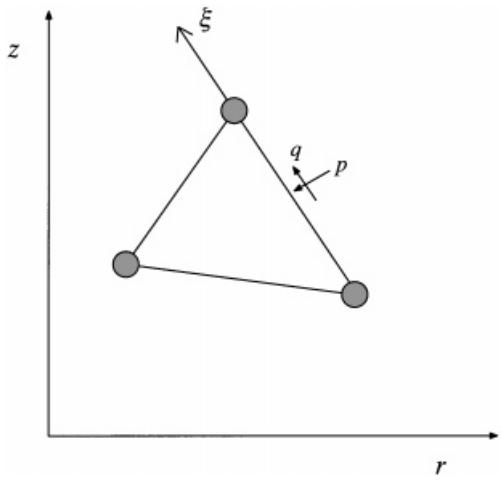

Figure 4. Calculation of nodal force vectors due to distributed surface tractions.

IMPLEMENTATION IN A STANDARD DISPLACEMENT FINITE ELEMENT PROGRAM

This section details the way by which the new element formulations described in the previous section can be implemented in a standard finite element program. Specific examples of where the modification is needed to the conventional finite element code are given below.

Discretization of region and transformation of co-ordinates

The new finite element formulations presented in this paper are based on the use of the generalized co-ordinates (R, z), where $R = r^2$. Thus, any mesh to be analysed with the new displacement interpolation functions must first be transformed into the generalized co-ordinates. Although two alternatives exist (e.g. [15]), the following method, that has been found to be entirely satisfactory and also very easy to implement, will be used in this study:

(1) For each element, the corner nodes are directly transformed from (r, z) space to (R, z) space.
(2) The remaining boundary are then positioned in (R, z) co-ordinates so that they are linearly equidistant between corner nodes.
(3) Any remaining internal nodes are positioned so that they are linearly equidistant between relevant boundary nodes.

The effect of this transformation is to generate straight-sided triangular or rectangular elements, rather than curved-sided elements in the generalized (R, z) space. This is desirable as the element stiffness matrix, as defined by Equation (31), should be calculated using an element geometry defined in the generalized co-ordinates (R, z).

Modifications to element stiffness matrix calculation

Conventional element stiffness matrix. For axisymmetric loading, the element stiffness is calculated by the following equation:

$$\mathbf{K} = 2\pi \iint_{(\alpha,\beta)} \mathbf{r}\mathbf{B}^{\mathrm{T}}\mathbf{D}^{\mathrm{ep}}\mathbf{B} \det J \, \mathrm{d}\alpha \, \mathrm{d}\beta \tag{35}$$

where the conventional strain–displacement matrix $\mathbf{B}$ is of the form

$$\mathbf{B} = \begin{bmatrix} \dfrac{\partial N_1}{\partial r} & 0 & \cdots & \dfrac{\partial N_{\mathrm{nd}}}{\partial r} & 0 \\ 0 & \dfrac{\partial N_1}{\partial z} & \cdots & 0 & \dfrac{\partial N_{\mathrm{nd}}}{\partial z} \\ \dfrac{\partial N_1}{\partial z} & \dfrac{\partial N_1}{\partial r} & \cdots & \dfrac{\partial N_{\mathrm{nd}}}{\partial z} & \dfrac{\partial N_{\mathrm{nd}}}{\partial r} \\ \dfrac{N_1}{r} & 0 & \cdots & \dfrac{N_{\mathrm{nd}}}{r} & 0 \end{bmatrix} \tag{36}$$

The calculations are performed based on the element geometries in the original co-ordinates (r, z).

New element stiffness matrix. The new element stiffness is calculated by equation (31):

$$\mathbf{K}_n = \pi \iint_{(\alpha,\beta)} \mathbf{B}_n^{\mathrm{T}}\mathbf{D}^{\mathrm{ep}}\mathbf{B}_n \det J \, \mathrm{d}\alpha \, \mathrm{d}\beta$$

where the new strain–displacement matrix $\mathbf{B}_n$ is given by equation (25):

$$\mathbf{B}_n = \begin{bmatrix} \dfrac{\partial \bar{N}_1}{\partial r} & 0 & \cdots & \dfrac{\partial \bar{N}_{\mathrm{nd}}}{\partial r} & 0 \\ 0 & \dfrac{\partial N_1}{\partial z} & \cdots & 0 & \dfrac{\partial N_{\mathrm{nd}}}{\partial z} \\ \dfrac{\partial \bar{N}_1}{\partial z} & \dfrac{\partial N_1}{\partial r} & \cdots & \dfrac{\partial \bar{N}_{\mathrm{nd}}}{\partial z} & \dfrac{\partial N_{\mathrm{nd}}}{\partial r} \\ \dfrac{\bar{N}_1}{r} & 0 & \cdots & \dfrac{\bar{N}_{\mathrm{nd}}}{r} & 0 \end{bmatrix}$$

It should be stressed that the calculations for the element stiffness in the new formulations are performed based on the element geometries in the generalized co-ordinates (R, z).

Modifications to nodal force vector calculation

The expressions for calculating nodal forces due to residual stresses, body forces and surface tractions are given by Equations (32)–(34), respectively. Since the surface tractions will be used later in this paper, the modifications required to calculate the nodal forces due to the surface tractions are given here.

For an application of distributed loads on an element edge, it is necessary to determine the components of the applied forces at each of nodes along that edge and then assemble each load into the global nodal force vector.

Conventional formulation of nodal force vector due to surface tractions. In the conventional formulation of the nodal force vector due to distributed loads, the nodal force vector due to the surface shear and normal tractions of q and p is given by

$$\mathbf{P}_s^e = 2\pi \int_\xi \mathbf{N}^{\mathrm{T}} r \begin{bmatrix} q\dfrac{\partial r}{\partial \xi} - p\dfrac{\partial z}{\partial \xi} \\ q\dfrac{\partial z}{\partial \xi} + p\dfrac{\partial r}{\partial \xi} \end{bmatrix} \mathrm{d}\xi \tag{37}$$

Note that the nodal force vector on the left-hand side of the above equation is defined by Equation (30), and the shape function matrix $\mathbf{N}$ contains the conventional shape functions.

New formulation of nodal force vector due to surface tractions. In the new formulation of the nodal force vector due to distributed loads, the nodal force vector due to the surface tractions (q, p) is given by Equation (34):

$$\mathbf{P}_s^e = 2\pi \int_\xi \mathbf{N}_n^{\mathrm{T}} r \begin{bmatrix} \dfrac{q}{2r}\dfrac{\partial R}{\partial \xi} - p\dfrac{\partial z}{\partial \xi} \\ q\dfrac{\partial z}{\partial \xi} + \dfrac{p}{2r}\dfrac{\partial R}{\partial \xi} \end{bmatrix} \mathrm{d}\xi$$

where the shape function matrix $\mathbf{N}_n$ contains the modified shape functions. For simplicity, the above equation may also be expressed in terms of the conventional shape functions and in a similar form as (37):

$$\mathbf{P}_s^e = 2\pi \int_\xi \mathbf{N}^{\mathrm{T}} r \begin{bmatrix} \dfrac{r_i}{r}\left(\dfrac{q}{2r}\dfrac{\partial R}{\partial \xi} - p\dfrac{\partial z}{\partial \xi}\right) \\ q\dfrac{\partial z}{\partial \xi} + \dfrac{p}{2r}\dfrac{\partial R}{\partial \xi} \end{bmatrix} \mathrm{d}\xi \tag{38}$$

where i denotes the node number along the element side with applied surface shear and normal tractions of q and p.

Summary of the necessary modifications

To implement the new finite element formulations into a standard displacement finite element program, the following changes are required:

(1) Discretization of meshes into the generalized co-ordinates (R, z).
(2) Modification to the expression for calculating element stiffness matrix.
(3) Modification to the expression for calculating nodal force vectors.

As can be seen in this section, the overall changes to a standard finite element program are not extensive and numerical implementation of the new formulations is therefore relatively straight forward.

NUMERICAL EXAMPLES

In this section, some numerical results are presented to illustrate the performance of the conventional and modified displacement finite elements for axisymmetric stress analysis of incompressible materials. A thick-walled cylinder subject to an uniform internal pressure has been used as the test problem, mainly because exact solutions are available for stress distributions which can be used to compare with the finite element results. The material will be modelled as either a purely elastic or an elastic–plastic material.

Expansion of a thick cylinder in an elastic incompressible material

This example is concerned with the detailed analysis of the stresses within an elastic thick cylinder subject to internal pressure, where the numerical stresses from both conventional and modified formulations are compared with the closed-form solutions given by Hill [18].

Six meshes of different element types with same or similar number of degrees of freedom shown in Figures 5–10 will be used in the analysis so that the performance of different elements can be compared. The geometry of the cylinder is defined by a value of the radio of external to internal

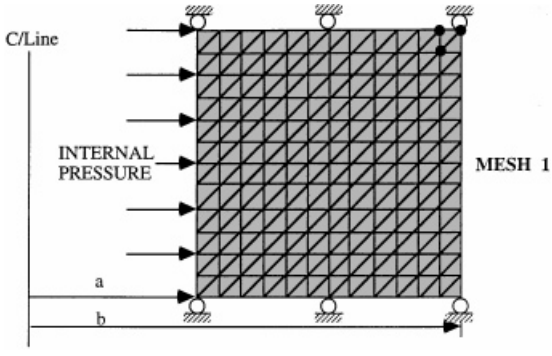

Figure 5. Mesh 1: mesh arrangement for cylinder expansion with 3-noded triangles.

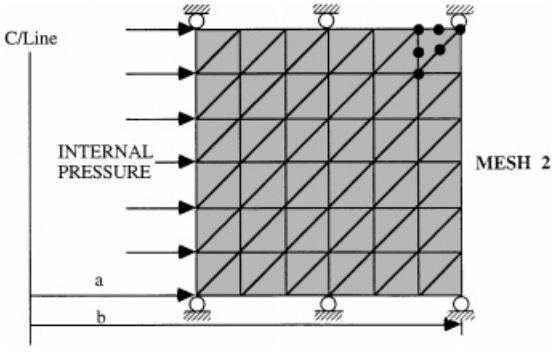

Figure 6. Mesh 2: mesh arrangement for cylinder expansion with 6-noded triangles.

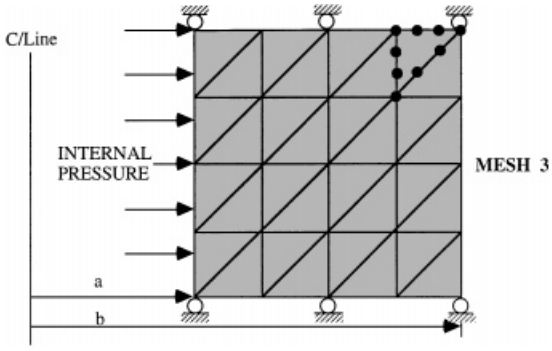

Figure 7. Mesh 3: mesh arrangement for cylinder expansion with 10-noded triangles.

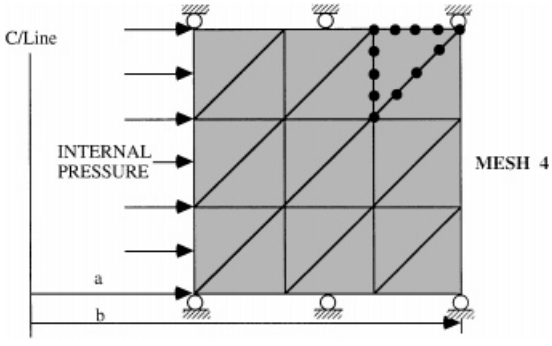

Figure 8. Mesh 4: mesh arrangement for cylinder expansion with 15-noded triangles.

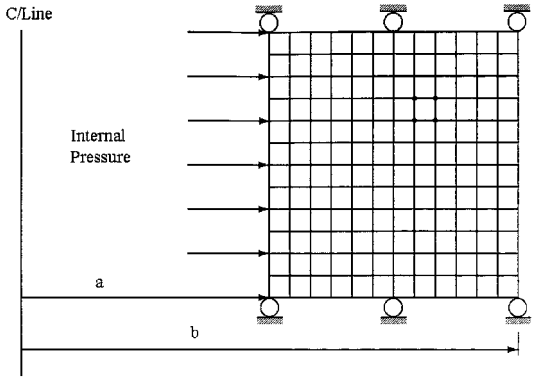

Figure 9. Mesh 5: mesh arrangement for cylinder expansion with 4-noded rectangles.

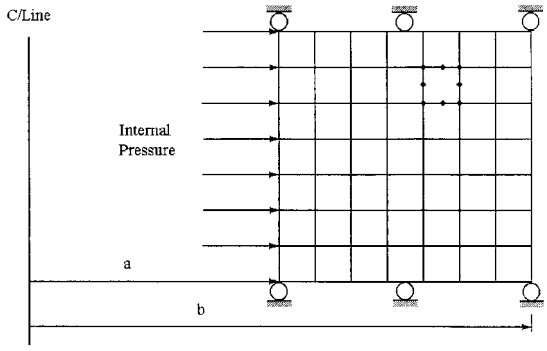

Figure 10. Mesh 6: mesh arrangement for cylinder expansion with 8-noded rectangles.

radii of 2. Specifically, Meshes 1–4 consist of 3, 6, 10 and 15-noded triangular elements, respectively, and have the same number of degrees of freedom of 169. Meshes 5 and 6 are arranged with the 4- and 9-noded rectangular elements and the number of degrees of freedom for Meshes 5 and 6 is equal to 176.

A series of analyses have been carried out for each mesh with both conventional and modified displacement interpolation functions. In the elastic analyses, six different ratios of the bulk modulus, K, to the shear modulus, G, are used to illustrate the behaviour of the different elements as material incompressibility is approached. For each of the element types, different integration rules are used in the calculation to observe the effect of reduced integration.

In order to assess the quality of the calculated stresses, an RMS error is calculated for each analysis. The percentage RMS errors, for both radial and hoop stresses, are defined as

$$e_r = 100 \times \left[\frac{1}{n} \sum_{i=1}^{i=n} \left(\frac{\sigma_{ri}^* - \sigma_{ri}}{p_{in}} \right)^2 \right]^{1/2} \tag{39}$$

$$e_\theta = 100 \times \left[\frac{1}{n} \sum_{i=1}^{i=n} \left(\frac{\sigma_{\theta i}^* - \sigma_{\theta i}}{p_{in}} \right)^2 \right]^{1/2} \tag{40}$$

where p_{in} is the applied internal pressure; σ_{ri}^* and $\sigma_{\theta i}^*$ are the radial and hoop stresses obtained from the finite element solution at Gauss point i; σ_{ri} and $\sigma_{\theta i}$ are the exact values of the radial and hoop stresses at Gauss point i and n is the total number of Gauss points in the mesh.

Results of the rms errors for Meshes 1–6 with both conventional and modified displacement interpolation functions are presented in Tables V–X, respectively. The observation of these results can be summarized as follows.

Effect of incompressibility and element types. For the elements based on the conventional displacement interpolation functions, the rms errors increase rapidly as the value of Poisson's ratio approaches 0.5. When Poisson's ratio is equal to 0.499995, the rms errors from the 3, 6- and 10-noded triangular elements and the 4- and 8-noded rectangular elements are in the order of 1000–10 000 per cent. In contrast, the 15-noded triangular element performed significantly better with typical rms errors of 300 per cent when the 'full integration' is used.

Table IV. Results of RMS errors for elastic analysis of cylinder expansion with Mesh 1 (where M indicates that Yu's modified displacement interpolation is used).

Mesh	nd	N_g	$K/G = 1$ ($v = 0.125$)		$K/G = 10$ ($v = 0.452$)		$K/G = 100$ ($v = 0.495$)		$K/G = 1000$ ($v = 0.4995$)		$K/G = 10000$ ($v = 0.49995$)		$K/G = 100000$ ($v = 0.499995$)	
			RMS error %		RMS error %		RMS error %		RMS error %		RMS error %		RMS error %	
			e_r	e_θ	e_r	e_θ	e_r	e_θ	e_r	e_θ	e_r	e_θ	e_r	e_θ
1	3	1	1.8	0.3	8.5	6.9	53.1	51.7	155.7	154.6	202.3	201.2	209.0	208.0
1	3	3	3.3	0.5	15.5	12.7	123.3	120.4	895.8	892.2	3366.6	3361.1	5049.7	5043.2
1	3	6	3.6	0.5	17.0	13.9	136.8	133.7	1011.4	1007.4	3809.3	3803.1	5713.8	5706.7
1	3	7	3.4	0.5	16.1	13.2	129.3	126.3	947.1	943.3	3562.8	3557.0	5343.6	5336.9
1	3	12	3.5	0.5	16.7	13.7	134.7	131.6	993.2	989.3	3739.8	3733.7	5609.4	5602.3
1	3	16	3.7	0.5	17.7	14.5	143.4	140.1	1066.4	1062.3	4202.1	4013.6	6030.3	6022.7
1	3	25	3.7	0.5	17.6	14.4	142.7	139.4	1060.8	1056.7	3998.7	3992.3	5998.2	5990.8
1(M)	3	1	0.2	0.2	0.3	0.2	0.3	0.2	0.5	0.4	0.6	0.5	0.6	0.6
1(M)	3	3	<0.05	<0.05	<0.05	<0.05	<0.05	<0.05	<0.05	<0.05	<0.05	<0.05	<0.05	<0.05
1(M)	3	6	<0.05	<0.05	<0.05	<0.05	<0.05	<0.05	<0.05	<0.05	<0.05	<0.05	<0.05	<0.05
1(M)	3	7	<0.05	<0.05	<0.05	<0.05	<0.05	<0.05	<0.05	<0.05	<0.05	<0.05	<0.05	<0.05
1(M)	3	12	<0.05	<0.05	<0.05	<0.05	<0.05	<0.05	<0.05	<0.05	<0.05	<0.05	<0.05	<0.05
1(M)	3	16	<0.05	<0.05	<0.05	<0.05	<0.05	<0.05	<0.05	<0.05	<0.05	<0.05	<0.05	<0.05
1(M)	3	25	<0.05	<0.05	<0.05	<0.05	<0.05	<0.05	<0.05	<0.05	<0.05	<0.05	<0.05	<0.05

Table V. Results of RMS errors for elastic analysis of cylinder expansion with Mesh 2 (where M indicates that Yu's modified displacement interpolation is used).

Mesh	nd	N_g	$K/G = 1$ ($v = 0.125$)		$K/G = 10$ ($v = 0.452$)		$K/G = 100$ ($v = 0.495$)		$K/G = 1000$ ($v = 0.4995$)		$K/G = 10000$ ($v = 0.49995$)		$K/G = 100000$ ($v = 0.499995$)	
			RMS error %		RMS error %		RMS error %		RMS error %		RMS error %		RMS error %	
			e_r	e_θ	e_r	e_θ	e_r	e_θ	e_r	e_θ	e_r	e_θ	e_r	e_θ
2	6	3	0.2	0.0	0.7	0.5	2.8	2.7	4.8	4.7	5.2	5.1	5.2	5.1
2	6	6	0.3	0.0	1.6	1.3	12.5	12.2	120.2	119.9	1094.5	1039.6	7940.5	7936.8
2	6	7	0.3	0.1	1.6	1.3	12.4	12.1	115.7	115.4	1077.8	1077.2	8048.1	8046.2
2	6	12	0.4	0.1	1.7	1.4	13.5	13.2	128.2	127.8	1174.5	1173.7	8602.6	8599.6
2	6	16	0.4	0.1	1.8	1.5	14.7	14.4	140.5	140.1	1300.1	1298.9	9616.8	9612.2
2	6	25	0.4	0.1	1.8	1.5	15.3	15.0	148.1	147.6	1341.8	1340.7	9693.7	9689.3
2(M)	6	3	0.1	<0.05	0.1	0.1	0.1	0.1	0.1	0.1	0.1	0.1	0.1	0.1
2(M)	6	6	<0.05	<0.05	<0.05	<0.05	<0.05	<0.05	<0.05	<0.05	<0.05	<0.05	<0.05	<0.05
2(M)	6	7	<0.05	<0.05	<0.05	<0.05	<0.05	<0.05	<0.05	<0.05	<0.05	<0.05	<0.05	<0.05
2(M)	6	12	<0.05	<0.05	<0.05	<0.05	<0.05	<0.05	<0.05	<0.05	<0.05	<0.05	<0.05	<0.05
2(M)	6	16	<0.05	<0.05	<0.05	<0.05	<0.05	<0.05	<0.05	<0.05	<0.05	<0.05	<0.05	<0.05
2(M)	6	25	<0.05	<0.05	<0.05	<0.05	<0.05	<0.05	<0.05	<0.05	<0.05	<0.05	<0.05	<0.05

Table VI. Results of RMS errors for elastic analysis of cylinder expansion with Mesh 3 (where M indicates that Yu's modified displacement interpolation is used).

Mesh	nd	N_g	$K/G = 1$ ($v = 0.125$)		$K/G = 10$ ($v = 0.452$)		$K/G = 100$ ($v = 0.495$)		$K/G = 1000$ ($v = 0.4995$)		$K/G = 10000$ ($v = 0.49995$)		$K/G = 100000$ ($v = 0.499995$)	
			RMS error %		RMS error %		RMS error %		RMS error %		RMS error %		RMS error %	
			e_r	e_θ	e_r	e_θ	e_r	e_θ	e_r	e_θ	e_r	e_θ	e_r	e_θ
3	10	6	<0.05	<0.05	0.1	0.1	2.2	2.2	0.4	0.3	0.4	0.4	0.4	0.4
3	10	7	<0.05	<0.05	0.1	0.1	0.8	0.8	7.7	7.6	59.5	59.5	241.8	241.8
3	10	12	0.1	<0.05	0.2	0.2	1.9	1.9	18.5	18.5	170.3	170.2	1285.2	1285.1
3	10	16	0.1	<0.05	0.3	0.2	2.3	2.2	21.7	21.7	199.2	199.2	1501.0	1500.9
3	10	25	0.1	<0.05	0.3	0.2	2.6	2.5	25.3	25.2	229.5	229.4	1673.0	1672.8
3(M)	10	6	<0.05	<0.05	<0.05	<0.05	0.1	0.1	0.1	0.1	0.1	0.1	0.1	0.1
3(M)	10	7	<0.05	<0.05	<0.05	<0.05	<0.05	<0.05	<0.05	<0.05	<0.05	<0.05	<0.05	<0.05
3(M)	10	12	<0.05	<0.05	<0.05	<0.05	<0.05	<0.05	<0.05	<0.05	<0.05	<0.05	<0.05	<0.05
3(M)	10	16	<0.05	<0.05	<0.05	<0.05	<0.05	<0.05	<0.05	<0.05	<0.05	<0.05	<0.05	<0.05
3(M)	10	25	<0.05	<0.05	<0.05	<0.05	<0.05	<0.05	<0.05	<0.05	<0.05	<0.05	<0.05	<0.05

Table VII. Results of RMS errors for elastic analysis of cylinder expansion with Mesh 4 (where M indicates that Yu's modified displacement interpolation is used).

MESH	nd	N_g	$K/G = 1$ ($\upsilon = 0.125$)		$K/G = 10$ ($\upsilon = 0.452$)		$K/G = 100$ ($\upsilon = 0.495$)		$K/G = 1000$ ($\upsilon = 0.4995$)		$K/G = 10000$ ($\upsilon = 0.49995$)		$K/G = 100000$ ($\upsilon = 0.499995$)	
			RMS error %											
			e_r	e_θ	e_r	e_θ	e_r	e_θ	e_r	e_θ	e_r	e_θ	e_r	e_θ
4	15	6	0.7	1.9	0.8	1.9	0.8	2.0	0.8	2.0	0.8	2.0	0.8	2.0
4	15	7	0.1	0.5	0.1	0.5	0.1	0.6	0.1	0.6	0.1	0.6	0.1	0.6
4	15	12	0.0	0.0	0.0	0.0	0.2	0.1	1.5	1.5	12.5	12.5	57.3	57.3
4	15	16	0.0	0.0	0.1	0.0	0.4	0.4	4.1	4.1	39.0	39.0	287.7	287.7
4	15	25	0.0	0.0	0.1	0.0	0.5	0.5	5.0	5.0	44.7	44.7	307.9	307.9
4(M)	15	6	2.7	9.9	2.8	10.1	2.9	10.1	2.9	10.2	2.9	10.2	2.9	10.2
4(M)	15	7	0.9	4.3	0.6	4.6	0.6	4.7	0.6	4.7	0.6	4.7	0.6	4.7
4(M)	15	12	<0.05	<0.05	<0.05	<0.05	<0.05	<0.05	<0.05	<0.05	<0.05	<0.05	<0.05	<0.05
4(M)	15	16	<0.05	<0.05	<0.05	<0.05	<0.05	<0.05	<0.05	<0.05	<0.05	<0.05	<0.05	<0.05
4(M)	15	25	<0.05	<0.05	<0.05	<0.05	<0.05	<0.05	<0.05	<0.05	<0.05	<0.05	<0.05	<0.05

Table VIII. Results of RMS errors for elastic analysis of cylinder expansion with Mesh 5 (where M indicates that Yu's modified displacement interpolation is used).

Mesh	nd	N_g	$K/G = 1$ ($v = 0.125$)		$K/G = 10$ ($v = 0.452$)		$K/G = 100$ ($v = 0.495$)		$K/G = 1000$ ($v = 0.4995$)		$K/G = 10000$ ($v = 0.49995$)		$K/G = 100000$ ($v = 0.499995$)	
			RMS error %											
			e_r	e_θ	e_r	e_θ	e_r	e_θ	e_r	e_θ	e_r	e_θ	e_r	e_θ
5	4	4	4.19	0.65	16.28	13.40	137.66	134.65	1036.9	1032.50	3072.60	3065.00	3824.70	3816.0
5	4	9	4.48	0.68	17.81	14.66	150.86	147.56	1136.2	1131.40	3366.30	3358.10	4190.10	4180.60
5	4	16	4.60	0.70	18.42	15.16	156.16	152.75	1176.2	1171.20	3484.80	3476.30	4337.50	4327.70
5	4	25	4.66	0.71	18.76	15.43	159.03	155.55	1197.8	1192.70	1548.80	3540.20	4417.30	4407.30
5(M)	4	4	2.61	0.44	3.63	3.06	5.42	5.34	7.20	7.19	7.83	7.83	7.92	7.92
5(M)	4	9	2.68	4.45	3.84	3.24	5.82	5.74	7.78	7.77	8.48	8.48	8.58	8.58
5(M)	4	16	2.70	4.49	3.92	3.31	5.99	5.90	8.02	8.01	8.75	8.75	8.85	8.85
5(M)	4	25	2.72	4.51	3.97	3.35	6.08	5.99	8.15	8.14	8.89	8.89	8.99	8.99

Table IX. Results of RMS errors for elastic analysis of cylinder expansion with Mesh 6 (where M indicates that Yu's modified displacement interpolation is used).

Mesh	nd	N_g	$K/G = 1$ ($v = 0.125$)		$K/G = 10$ ($v = 0.452$)		$K/G = 100$ ($v = 0.495$)		$K/G = 1000$ ($v = 0.4995$)		$K/G = 10000$ ($v = 0.49995$)		$K/G = 100000$ ($v = 0.499995$)	
			RMS error %											
			e_r	e_θ	e_r	e_θ	e_r	e_θ	e_r	e_θ	e_r	e_θ	e_r	e_θ
6	8	4	0.38	0.1	0.4	0.26	0.46	0.38	0.63	0.58	0.82	0.78	0.90	0.87
6	8	9	0.25	0.1	1.20	0.98	9.57	9.35	76.51	76.27	699.03	698.57	5921.30	5919.00
6	8	16	0.29	0.1	1.35	1.11	10.82	10.57	86.35	86.08	790.57	790.0	6693.90	6691.00
6	8	25	0.30	0.1	1.42	1.16	11.40	11.14	91.81	91.52	848.3	847.7	7257.70	7254.30
6	8	4	0.59	0.1	0.63	0.42	0.73	0.61	1.02	0.94	1.33	1.28	1.45	1.40
6	8	9	<0.05	<0.05	<0.05	<0.05	<0.05	<0.05	<0.05	<0.05	<0.05	<0.05	<0.05	<0.05
6	8	16	<0.05	<0.05	<0.05	<0.05	<0.05	<0.05	<0.05	<0.05	<0.05	<0.05	<0.05	<0.05
6	8	25	<0.05	<0.05	<0.05	<0.05	<0.05	<0.05	<0.05	<0.05	<0.05	<0.05	<0.05	<0.05

Table X. Results of RMS errors for elastic–plastic analysis of cylinder expansion with Meshes 1–6 (where M indicates that Yu's modified displacement interpolation is used).

Mesh	nd	N_g	$K/G = 1$ ($v = 0.125$)		$K/G = 100$ ($v = 0.495$)		$K/G = 1000$ ($v = 0.499995$)	
			RMS error %		RMS error %		RMS error %	
			e_r	e_θ	e_r	e_θ	e_r	e_θ
1	3	1	2.4	2.4	53.3	52.6	188.5	188.0
1	3	3	4.2	3.5	128.0	126.7	5049.6	5045.6
1(M)	3	1	1.1	1.1	0.6	0.6	0.9	0.9
1(M)	3	3	1.8	1.8	1.6	1.7	1.5	1.5
2	6	3	0.2	0.2	2.8	2.7	5.1	5.0
2	6	6	0.4	0.3	13.2	13.1	7951.4	7948.3
2(M)	6	3	0.1	0.1	0.2	0.2	0.2	0.3
2(M)	6	6	0.1	0.2	0.3	0.4	0.4	0.4
3	10	6	0.2	0.2	0.4	0.4	0.6	0.5
3	10	12	0.6	0.5	1.6	1.6	1306.1	1306.3
3	10	16	0.6	0.4	2.0	2.0	1526.2	1526.3
3	10	25	0.5	0.4	2.4	2.3	1696.6	1696.9
3(M)	10	6	0.2	0.2	0.2	0.2	0.3	0.3
3(M)	10	12	0.6	0.5	0.5	0.5	0.5	0.5
3(M)	10	16	0.6	0.4	0.5	0.5	0.5	0.5
3(M)	10	25	0.5	0.5	0.5	0.5	0.6	0.6
4	15	6	1.2	3.8	1.2	3.8	1.2	3.8
4	15	12	0.4	0.5	0.3	0.3	57.2	57.3
4	15	16	0.8	0.5	0.5	0.5	294.1	294.2
4	15	25	0.7	0.4	0.4	0.5	311.8	311.9
4(M)	15	6	4.2	7.4	4.4	7.6	4.4	7.6
4(M)	15	12	0.6	0.5	0.5	0.5	0.5	0.6
4(M)	15	16	0.7	0.5	0.6	0.6	0.6	0.6
4(M)	15	25	0.6	0.4	0.5	0.5	0.5	0.5
5	4	4	6.01	8.00	142.41	141.54	3824.94	3819.23
5	4	9	6.35	8.17	155.98	155.04	4190.35	4184.25
5	4	16	6.49	8.26	161.41	160.40	4337.74	4331.44
5	4	25	6.57	8.27	164.44	163.41	4417.47	4411.08
5(M)	4	4	4.51	7.32	6.73	9.32	9.04	11.15
5(M)	4	9	4.64	7.38	7.10	9.56	9.70	11.65
5(M)	4	16	4.72	7.47	7.27	9.70	9.98	11.91
5(M)	4	25	4.75	7.46	7.38	8.29	10.13	12.04
6	8	4	3.15	6.92	3.17	7.01	3.32	7.09
6	8	9	3.20	7.10	10.96	12.12	6007.78	6004.00
6	8	16	3.23	7.14	12.37	13.08	6793.92	6788.99
6	8	25	3.26	7.10	13.04	13.47	7359.61	7354.03
6(M)	8	4	3.16	6.93	3.21	7.04	3.39	7.11
6(M)	8	9	3.12	7.08	3.12	7.14	3.13	7.14
6(M)	8	16	3.12	7.12	3.14	7.18	3.15	7.18
6(M)	8	25	3.15	7.07	3.15	7.14	3.23	7.17

On the other hand, when the modified displacement interpolation functions are used, the rms errors are largely independent of the value of Poisson's ratio (i.e. incompressibility). With the exception of the 4-noded rectangle (Mesh 5), the values of the rms error obtained from all the analyses are less than 0.05 per cent when the 'full integration' is used. This is in agreement with the theoretical prediction presented in Table III indicating that the 4-noded rectangle is not suitable for incompressible analysis even when the modified displacement interpolation functions are used.

Effect of integration schemes. For the meshes using the conventional displacement interpolation functions, the rms errors increase when the number of Gauss integration points increases. For example, when Poisson's ratio is equal to 0.499995, the rms errors from the 8-noded rectangular elements, when a 4-point integration (i.e. reduced integration) is used, are less than 1 per cent. In contrast, when a 9-point integration (i.e. full integration) is used, the rms errors are over 5900 per cent. The rms errors increase with the number of Gauss points used in the calculation of the element stiffness matrix. This suggests that although reduced integration may be used to improve the stresses at a fewer number of points within the element, it fails to satisfy the incompressibility condition everywhere in the element.

Although the rms errors for all the elements based on the modified displacement interpolation functions are very small, it is interesting to note that they tend to decrease slightly when the number of Gauss points increases. This is because that as the order of integration is increased, the element stiffness matrix is calculated increasingly more accurately without introducing additional incompressibility constraints. This is also a strong evidence that the incompressibility condition is satisfied everywhere in the element when the new displacement interpolation functions are used.

Expansion of a thick cylinder in an elastic-plastic incompressible material

This second example is concerned with the detailed analysis of the stresses within an elastic–plastic thick-walled cylinder subject to internal pressure. The numerical stresses from both conventional and modified formulations are compared with the closed-form solutions given by Hill [18]. The Tresca yield criterion is used to define the onset plastic yielding. For a cylinder with the ratio of external to internal radii of 2, the value of internal pressure at initial yielding is $0.75c$, where c is the cohesion of the material. The entire cylinder becomes plastic when the internal pressure is equal to $1.38c$. In this study, the stresses at each Gauss point when the internal pressure is equal to $0.95c$ are used to compare with the exact solutions.

Analyses have been carried out for Meshes 1–6 with both conventional and modified displacement interpolation functions. In the elastic–plastic analyses, three different ratios of the bulk modulus, K, to the shear modulus, G, are used to illustrate the behaviour of the different elements as material incompressibility is approached. For each of the element types, different integration rules are again used to observe the effect of reduced integration.

Elastic–plastic results in terms of the rms errors for Meshes 1–6 with both conventional and modified displacement interpolation functions are presented in Table X. Generally speaking, similar conclusions can be made for elastic–plastic analyses as those based on the results of the purely elastic analyses presented earlier.

CONCLUSIONS

The theoretical criterion originally developed by Nagtegaal *et al.* [4] has been used to assess the suitability of displacement finite elements when used to analyse incompressible materials. It was

found that the 3-, 6-, 10-, 15-noded triangular elements and the 8-noded rectangle are able to satisfy the Nagtegaal criterion under axisymmetric loading conditions provided that the new displacement interpolation functions proposed by Yu [13,14] are used.

Based on Yu's new displacement interpolation functions, this paper presents a general isoparametric finite element formulation that can be used to implement into various triangular and rectangular displacement elements. More importantly, it has been shown that the new formulations can be readily implemented in an existing displacement-based finite element program, with only few changes to expressions for the shape function matrix and nodal force vectors.

The results of the numerical analyses of both elastic and elastic–plastic incompressible behaviour confirm the theoretical predictions. A detailed comparison between the numerical and analytical stresses indicates that when the incompressibility condition is approached, most conventional displacement finite elements failed completely in predicting the stresses. On the other hand, in agreement with the theoretical prediction, the numerical analyses suggest that the new finite element formulations based on Yu's displacement interpolation functions leads to a very high accuracy in the calculated stresses.

REFERENCES

1. Herrmann LR. Elasticity equations for incompressible and nearly incompressible materials by a variational theorem. *Journal of American Institute for Aeronautics and Astronautics* 1965; **3**:1896–1900.
2. Christian JT. Undrained stress distribution by numerical methods. *Journal of Soil Mechanics and Foundation Division ASCE* 1968; **96**:1289–1310.
3. Naylor DJ. Stresses in nearly incompressible materials by finite elements with application to the calculation of excess pore pressures. *International Journal for Numerical Methods in Engineering* 1974; **8**:443–460.
4. Nagtegaal JC, Parks DM, Rice JR. On numerically accurate finite element solutions in the fully plastic range. *Computational Methods in Applied Mechanics and Engineering* 1974; **4**:153–177.
5. Zienkiewicz OC, Taylor RL, Too TM. Reduced integration technique in general analysis of plates and shells. *International Journal for Numerical Methods in Engineering* 1971; **3**:275–290.
6. Burd HJ, Houlsby GT. Finite element analysis of two cylindrical expansion problems involving near incompressible material behaviour. *International Journal for Numerical and Analytical Methods in Geomechanics*. 1990; **14**:351–366.
7. Sloan SW, Randolph MF. Numerical prediction of collapse loads using finite element methods. *International Journal for Numerical and Analytical Methods in Geomechanics* 1982; **6**:47–76.
8. Malkus DS, Hughes TJR. Mixed finite element method—reduced and selective integration techniques: a unification of concepts. *Computational Methods in Applied Mechanics & Engineering* 1978; **15**:63–81.
9. Sloan SW, Randolph MF. Discussion on 'Elasto-plastic analysis of deep foundations in cohesive solids' by D.V. Griffiths. *International Journal for Numerical and Analytical Methods in Geomechanics*. 1983; **7**:385–393.
10. Naylor DJ. On integrating rules for triangles. *Numerical Methods in Geotechnical Engineering*, Smith (ed.), Balkema: Rotterdam. 1994; 111–114.
11. Sloan SW. Numerical analysis of incompressible and plastic solids using finite elements. *Ph.D. Thesis*, University of Cambridge, England, 1981.
12. De Borst R, Vermeer PA. Possibilities and limitations of finite elements for limit analysis. Geotechnique. 1984; **34**:199–210.
13. Yu HS. Cavity expansion theory and its application to the analysis of pressuremeters. *DPhil. Thesis*, University of Oxford, England, 1990.
14. Yu HS. A rational displacement interpolation function for axisymmetric finite element analysis of incompressible materials. *Finite Elements in Analysis and Design* 1991; **10**:205–219.
15. Yu HS, Houlsby GT, Burd HJ. A novel isoparametric finite element displacement formulation for axisymmetric analysis of nearly incompressible materials. *International Journal for Numerical Methods in Engineering*. 1993; **36**:2453–2472.

16. Jinka AGK, Lewis RW. Incompressibility and axisymmetry: a modified mixed and penalty formulation. *International Journal for Numerical Methods in Engineering* 1994; **37**:1623–1649.
17. Laursen ME, Gellert M. Some criteria for numerically integrated matrices and quadrature formulas for triangles. *International Journal for Numerical Methods in Engineering* 1978; **12**:167–176.
18. Hill R. *The Mathematical Theory of Plasticity*. Oxford University Press: Oxford, 1950.

